Journal of Applied Polymer Science

In Situ Microscopic Infrared Imaging Study on Deformation-Induced Spatial Orientation and Phase Transition Distributions of PA12

Liang Chen, Wei Chen, Weiming Zhou, Jing Li, Yanping Liu, Zeming Qi, Liangbin Li
CAS Key Laboratory of Soft Matter Chemistry, National Synchrotron Radiation Lab and College of Nuclear Science and Technology, University of Science and Technology of China, Hefei, China
Correspondence to: Z. Qi (E-mail: zmqi@ustc.edu.cn)

ABSTRACT: The relationship of deformation-induced phase transition and orientation distributions of polyamide 12 in necking region is studied by *in situ* Fourier transformation infrared microspectroscopic imaging (FTIRI) under uniaxial tensile test. With the detection of an area of 250 × 250 μm^2 with 4096 Fourier transformation infraredspectra, the absorption distributions of crystal (1064 cm^{-1} band) and amorphous (1028 cm^{-1} band) phases with radiation polarized parallel and perpendicular to tensile direction are obtained, and the spatial orientation distributions in necking region as well as the yielding properties during necking propagation are analyzed. The results show that the crystal and amorphous are highly oriented and the spatial distributions are correlated with the necking propagation. The phase-transforming characteristics show that part of amorphous phase transforms to crystal phase and part of γ phase transforms to transient α'' phase in the necking region, which are also correlated with the necking propagation and drawing ratios. All these behaviors occur in the plastic deformation stage, which show a close correlation between the mechanical response and the structural evolution during uniaxial tensile deformation. © 2014 Wiley Periodicals, Inc. J. Appl. Polym. Sci. **2014**, *131*, 40703.

KEYWORDS: crystallization; mechanical properties; polyamides

Received 9 January 2014; accepted 2 March 2014
DOI: 10.1002/app.40703

INTRODUCTION

Nylons are important engineering materials and widely used in industry because of their excellent properties such as high-impact resistance, good mechanical properties, thermal stability, and good toughness.[1–8] The studies show that the hydrogen bonds constituted in the neighboring molecular chains, play the most important role in determining the crystal structures and the properties of nylons.[9–11] Deformation-induced crystal transformation is a common behavior of polyamide family and also play important factors on nylon properties.[12–21] Many studies have given detailed views of crystal transition properties and the main efforts are to establish the relationship between mechanical behaviors and deformation-induced orientations and phase transitions. For example, Starkweather et al.[22] studied the mechanical properties and crystallinity of PA 66 under uniformly tensile deformation at room temperature and found part of crystalline transformed into fiber structure with high orientation, Na et al.,[23,24] Pierron et al.,[25] and Vasanthan[26] observed that a great part of β phase of PA 6 transited into α phase under uniaxial drawing.

Similar to other semicrystalline polymers, PA12 also shows crystal-to-crystal transformation and necking properties under tensile deformation.[27,28] For PA12, there has four different crystal phases denoted as α, γ, α' and γ' forms which depend on crystallization conditions while γ form is the most common form with a hexagonal or sometimes pseudohexagonal packing with four repeating monomer unites, and is characterized with a strong diffraction peak with d spacing around 0.41–0.42 nm. The α form belongs to monoclinic system, which gives two diffraction peaks with d spacings of about 0.37 and 0.45 nm and can be obtained under the following conditions: crystallization or casting from solution, drawing just below the melting point, or crystallization under high pressure. The α' form can be observed near the melting temperature of PA12, which characterized by two diffraction peaks in wide angle X-ray scattering (WAXS), and are closer to each other than those of α phase. The γ' form has a similar WAXS pattern as that of γ form, which can transform to α phase through thermal treatment under pressure.[29–31]

Studies show that deformation-induced phase transition of PA12 is a complicated process. Ishikawa et al.[27] observed γ to α partial transformation in PA12 by drawing near the melting temperature, and the productions were highly relative to the drawing ratios and experimental temperatures. Our group[29] also studied the crystal transition properties of PA12 during drawing

and found that γ phase transforming to transient phase by drawing. Further studies showed that the transient phase finally transform to γ' phase with continuously drawing above the glass transition temperature. Bai et al.[31] studied the deformation-induced phase transitions of PA12 in its segmented copolymers with polytetrahydrofuran at different temperatures and also indicated that γ form transform to transient form. These give detailed evidences of phase transition processes of PA12 during tensile deformation and help to understand the mechanical characters and crystal-to-crystal behaviors of semicrystalline polymers.[32–34] Nevertheless to our knowledge, some studies continually concern on the relationship of crystal and amorphous spatial orientation distributions as well as the crystal transition in necking region during tensile deformation, which can provide direct evidences of the relationship of the mechanical characters and their superstructures of polyamide family.

In this work, the relationship of spatial orientation distributions and the crystal transition of PA12 in necking region during tensile deformation is studied *in situ* combining with a homemade miniature tensile tester and Fourier transform infrared spectroscopic imaging (FTIRI). FTIRI has the advantages in detecting the amorphous orientation as well as crystal orientation in microzone, which provides a valuable tool for studying the relationships of the orientation distributions and phase-transition behaviors of polymers in necking region, and gives a direct correlation between mechanical behaviors and structural evolution.[35–40]

EXPERIMENTAL

Material and Sample Preparation

PA12 granules used in the experiments are kindly supplied by Evonik Degussa with trade name of L 1600. The glass transition temperature and melting point are about 40 and 178°C, respectively. The PA12 was dried in vacuum at 65°C for 12 h and then compressed to a film with thickness about 96 μm by a compression molding at 185°C for 10 min and then erasing thermal history at 190°C for 5 min at nitrogen atmosphere. The films were cooled down to room temperature naturally and then cut into rectangular-shaped specimens with length and width of 12 and 3 mm, respectively, for uniaxial tensile test.

Tensile Test and *In Situ* FTIRI Measurement

A homemade miniature tensile tester combined with FTIRI was used to carry out the tensile test as described elsewhere.[33] Briefly, the rectangular-shaped samples are mounted between two clamps of the tensile tester, which then is installed on the sample platform of FTIRI. During the experiments, the PA12 films were drawn with a constant tensile speed of 0.03 mm/min at 25 ± 0.3°C. Because of the low elongation speed as well as the synchronized movement of the two clamps, the test can be treated as quasistatic process, during which the sampling region of FTIRI keeping relatively static.

In situ FTIRI measurements were carried out with an IFS66v Fourier transformation infrared (FTIR) spectrometer, an infrared microscope (HYPERION 3000), a 64 × 64 (4096) mercury cadmium telluride Focal Plane Array (FPA) detector and a Specac KRS5 polarizer. With the FPA detector, it allows to measure

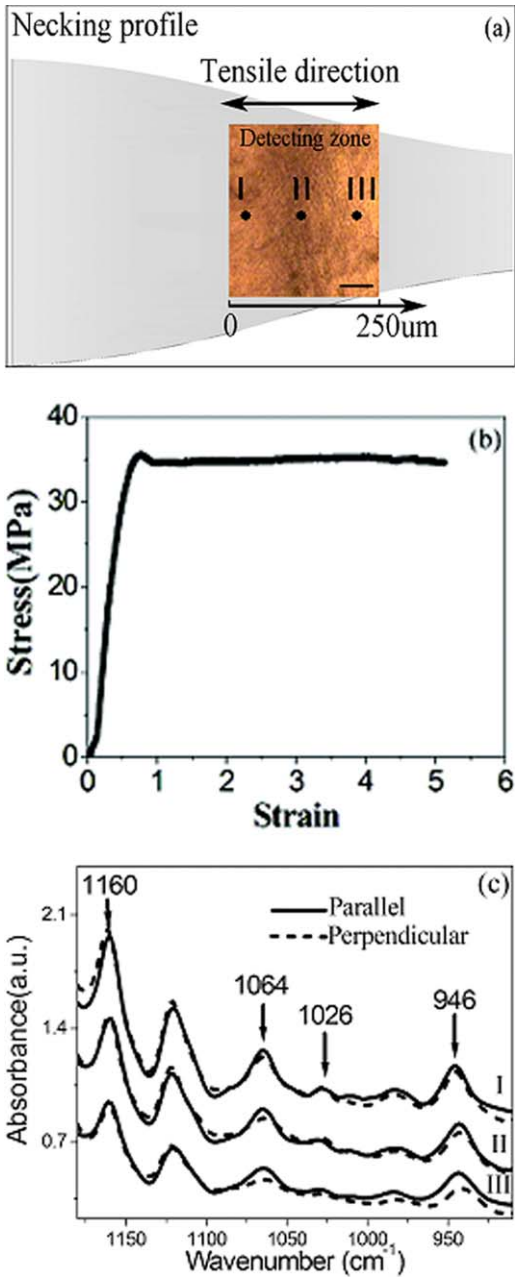

Figure 1. (a) The necking optical morphology of PA12 film after stretching and the sketch of selected zone for average orientation evolution in necking region, the scale bar is 50 μm, (b) the engineering stress–strain curve, and (c) corresponding FTIR spectra of Point I, II, and III in the fingerprint range of 1200–900 cm^{-1}. The black and dash lines are spectra with radiation polarized parallel and perpendicular to tensile direction, respectively. [Color figure can be viewed in the online issue, which is available at wileyonlinelibrary.com.]

4096 FTIR spectra in an area of 250 × 250 μm^2 simultaneously in transmission mode with a spatial resolution of 4 × 4 μm^2 and spectral range of 4000–800 cm^{-1}. With spectral resolution of 4 cm^{-1}, the 4096 spectra can be collected with 128 scans within 3.5 min. These spatial and time resolutions are well suitable to follow the spatial and time evolutions of the orientation distributions during tensile test.

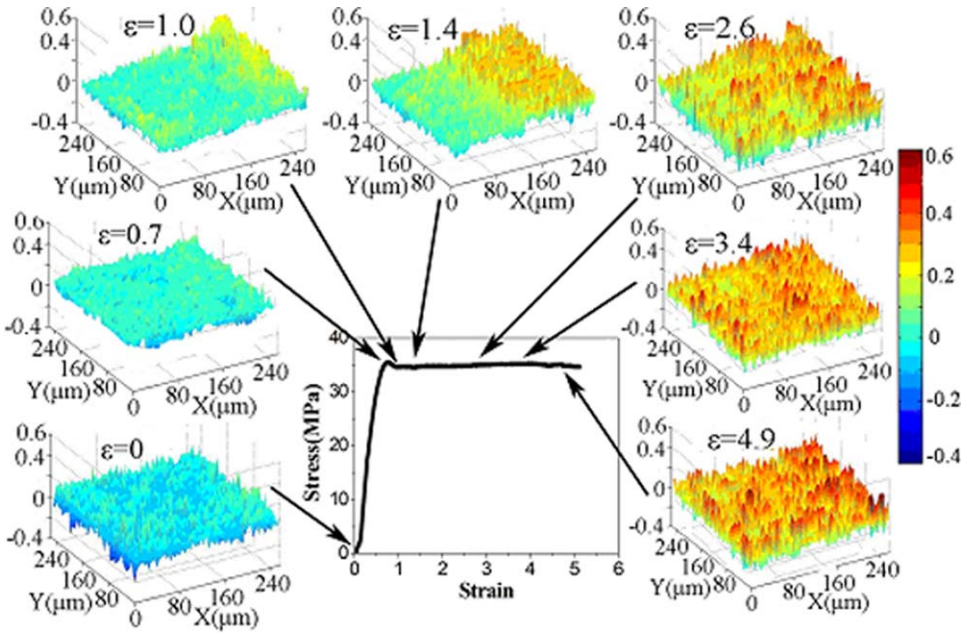

Figure 2. Engineering stress–strain curve and corresponding selected 2D crystal orientation distribution images of PA12 with different strains in the necking region. [Color figure can be viewed in the online issue, which is available at wileyonlinelibrary.com.]

For quantitative estimation of orientations, the intensity distribution images of interested absorption bands are obtained by integrating the heights of the corresponding peaks, and then the effect of anisotropy on a particular absorption band in infrared spectrum is defined as the dichroic ratio R:

$$R = A_{\parallel}/A_{\perp} \tag{1}$$

where $A_{\parallel}$ and $A_{\perp}$ are the integrated absorbance measured with radiations polarized parallel and perpendicular to the tensile direction, respectively.

Then, the degree of orientation f of crystal and amorphous can be further calculated by eq. (2)[33]

$$f = (R-1)/(R+2) \tag{2}$$

As the spectra are taken with polarized infrared radiation, the structural absorption is calculated with $A_0 = (A_{\parallel} + 2A_{\perp})/3$.

The crystallinity is estimated via a comparison of A_{crystal} and $A_{\text{amorphous}}$ with eq. (3),

$$X_{\text{cry}} = \frac{A_{\text{crystal}}}{A_{\text{crystal}} + A_{\text{amorphous}}} \times 100\% \tag{3}$$

RESULTS AND DISCUSSION

Spatial Orientation Distributions

Figure 1(a) is the necking propagation front viewed by optic microscope, and the corresponding engineering stress-strain

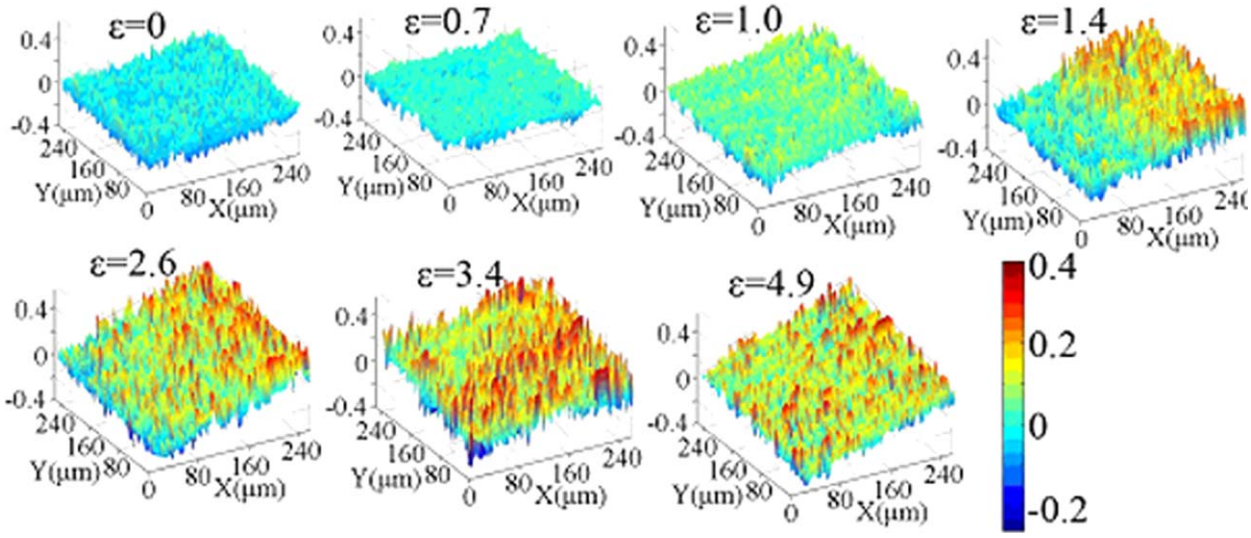

Figure 3. The selected 2D amorphous orientation distribution images of PA12 film with different strains in the necking region. [Color figure can be viewed in the online issue, which is available at wileyonlinelibrary.com.]

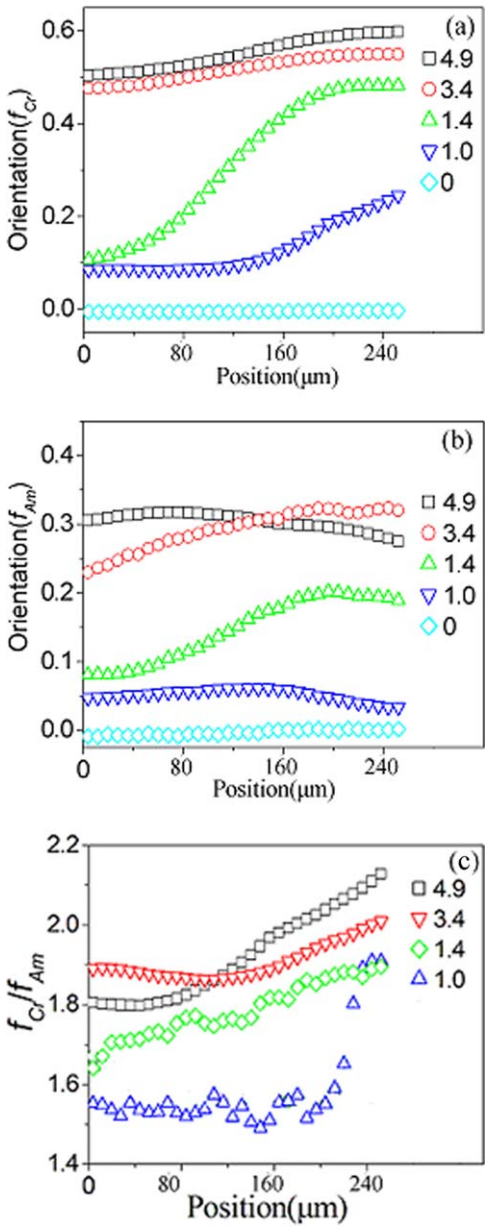

Figure 4. Average distributions of crystal (a), amphorous (b) orientations, and corresponding f_{Cr}/f_{Am} (c) of PA12 film in the necking region along the tensile direction. [Color figure can be viewed in the online issue, which is available at wileyonlinelibrary.com.]

curve in the tensile deformation is shown in Figure 1(b). The infrared spectra in the fingerprint range (1200–900 cm^{-1}) of the three selected zones in the necking region are listed in Figure 1(c). From the picture of Figure 1(a), the small spherulitic feature of the starting sample can be seen (the left side), while oriented fibrillar feature is observed in the right side. The small size of spherulites in the initial sample is an advantage for analysis, so that it can be treated as a homogeneous system with a resolution of several micrometers.

To construct the spatial distributions of crystal and amorphous orientations of PA12 during uniaxial stretching, FTIR spectra with radiation parallel and perpendicular to tensile directions at different drawing ratios are measured. Because the bands at 946, 980, and 1064 cm^{-1} are associated with the crystalline phase, while the bands at 1026 and 1160 cm^{-1} are associated with the amorphous phase.[41–43] As 1064 and 1026 cm^{-1} show strong dichroism, the vibrational bands at 1064 (CONH in-plane deformation) and 1026 cm^{-1} (skeletal motion involving CONH) are assigned as crystalline phase and amorphous phase for analyzing quantitative behaviors of the uniaxial orientation, respectively. Because the absorption is the strongest with radiation polarized parallel to chain axis,[44] the intensity of the absorption bands at 1064 and 1026 cm^{-1} with radiation polarized parallel (the black line) to tensile direction is larger than that in perpendicular direction (the dash line). With the equations (1) and (2), the dichroic ratios of 1064 and 1026 cm^{-1} bands, R_{1064} and R_{1026}, and the degree of orientation f of crystal and amorphous can be calculated, respectively.

The engineering stress–strain curve and the corresponding selected two-dimensional (2D) crystal, amorphous orientation distribution images with different strains during necking initiation, and propagation are shown in Figures 2 and 3, respectively. To give a close look at the changes of the axial distributions of crystal and amorphous orientations with different strains during tensile deformation, the orientation parameters are averaged over all the 64 points perpendicular to the tensile direction, which produce one-dimensional (1D)

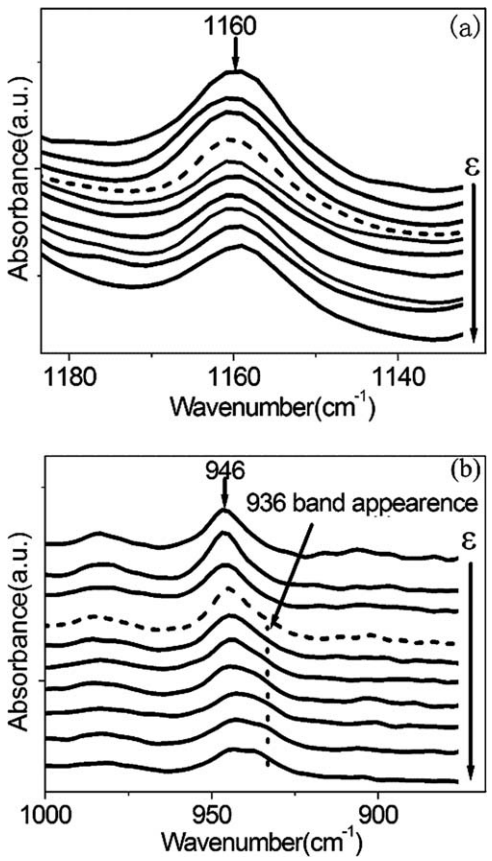

Figure 5. The 1160 cm^{-1} amorphous (a) and 946 cm^{-1} crystal (b) FTIR spectrum bands of the selected zone during tensile deformation, the small dashed line is corresponding to the yielding point.

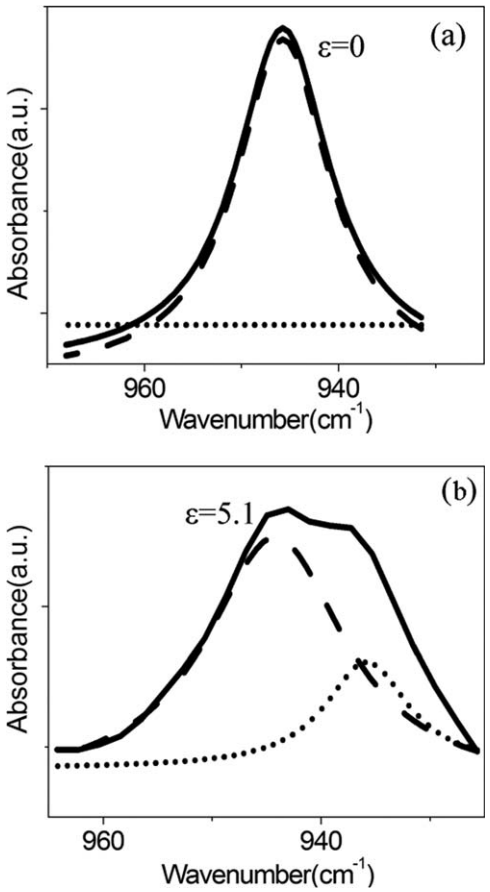

Figure 6. The crystal spectral band and the fitted 946 and 936 cm^{-1} bands at different strains, the black curve is the original crystal band, the small dot curve is 936 cm^{-1} band while the dash line is 946 cm^{-1} band. (a) $\varepsilon = 1.0$, (b) $\varepsilon = 5.1$.

orientation distributions along the neck propagating direction (as presented in Figure 4). The figures reveal that, at beginning the uniaxial deformation, the crystal orientation distributions are almost uniform with a value of about zero, which show that the film is isotropic at the beginning of stretching. When reaching at the yielding point, there has an increase of the crystal orientations (about 0.1 with strain of 0.7) but the whole images also show a rather uniform distribution. After passing the yielding point, there has a slightly decrease of stress and, then, neck forms, and the corresponding 2D distributions of crystal orientations become nonuniform. The average crystal orientation increases quickly up to 0.25 with strain of 1.0 in the necking region, while the non-necking region still keeps a relative low orientation. With strain increasing, the crystal 2D orientation distributions in the image increase and finally almost show a uniform distribution. The average orientation finally almost reaches to a plateau of 0.6 with strain of 4.9 as the necking region expanding to the whole detected region.

The amorphous orientation 2D distributions almost show same trends as the neck propagating into the observed region. However, the changes of amorphous orientation distributions show a little difference compared with that of crystal orientation. After increasing to the maximum about 0.46 with strain of 3.6, there has a slight decrease of amorphous orientation with strain increasing and the necking region expanding to the whole detected region, and finally about to 0.41 with strain of 4.9, which has about 0.05 decrease compared to the maximum amorphous orientation.

To evolute the relationship of crystal and amorphous orientation distributions under tensile deformation, the average crystal and amorphous orientations (f_{Cr}/f_{Am}) ratios of the detected region along the tensile direction are calculated for analyzing the changing trends directly [presented in Figure 4(c)]. The figures reveal that the orientations of crystal and amorphous phases increase mainly in the necking region. Once the neck propagating into the detected region, the crystal and amorphous orientations increase dramatically. The ratios of f_{Cr}/f_{Am} also shows a quick increase, which may reveal that crystal orientation increasing is quicker than amorphous orientation increasing during neck initiating and propagating. As the neck expanding to the whole observed region at high strains, f_{Cr}/f_{Am} increases almost linearly. The results indicate that crystal and amorphous orientations increasing are not synchronous and

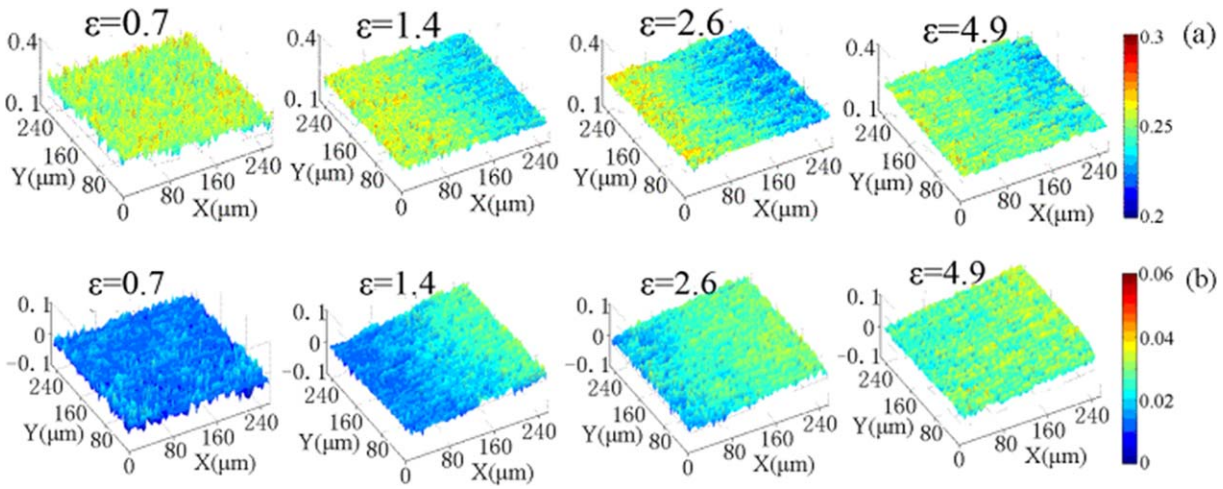

Figure 7. The selected 2D crystallinity distribution imagings of γ phase (a) and α'' phase (b) in the necking region. [Color figure can be viewed in the online issue, which is available at wileyonlinelibrary.com.]

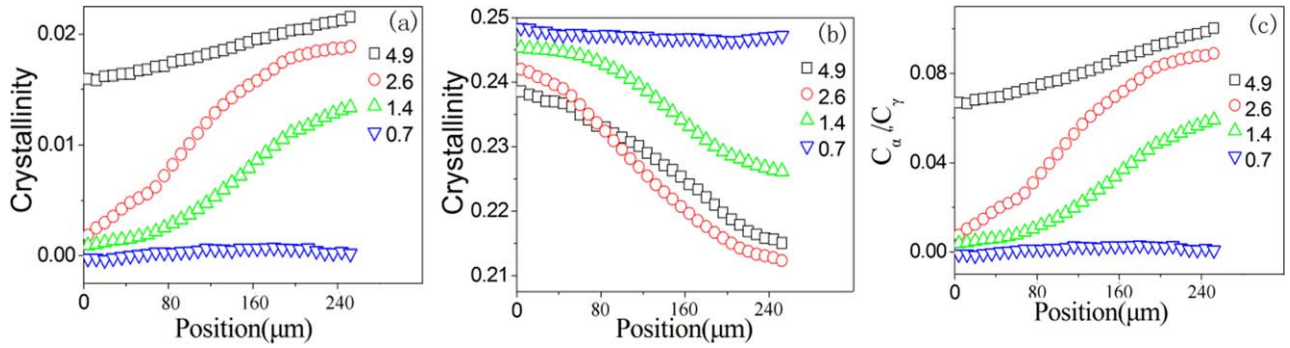

Figure 8. The selected average crystallinities of α'' phase (a), γ phase (b) and ratios ($C_{\alpha''}/C_\gamma$) of α'' and γ crystallinities with different drawing ratios during necking propagation. [Color figure can be viewed in the online issue, which is available at wileyonlinelibrary.com.]

amorphous orientation increasing is more slowly than crystal orientation increasing at high strains. The possible reasons are that amorphous phase transforms to crystal phase, which consumes oriented amorphous and lead to a reduction of amorphous orientation besides the highly oriented crystal chains along the tensile direction lead to a reduction of stress and causes amorphous chains to relax and lose part of initial orientation. The changes of orientation distributions reflect the kinetic process during necking propagation with time and indicate the relationship of amorphous phase transforming to crystal phase, which is coincident with the observation in stretching-induced recrystallization of polymer such as isotactic polypropylene.[34]

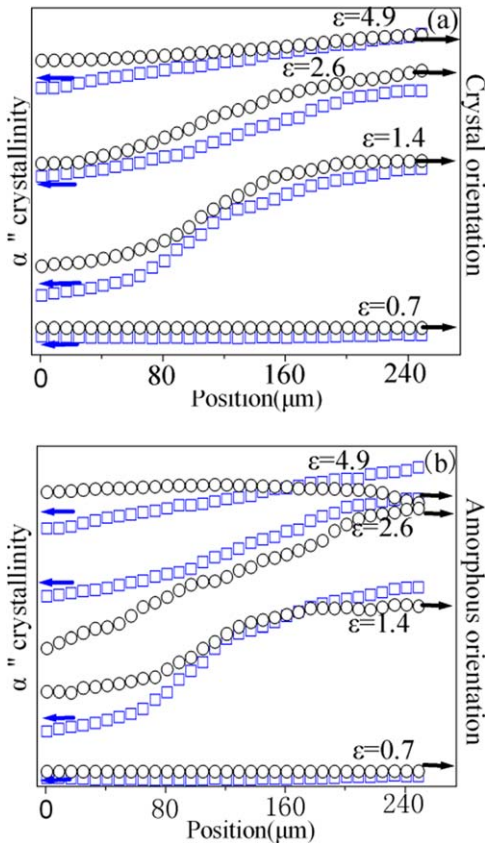

Figure 9. The changing trends of average α'' crystallinities compared with average crystal, amorphous orientations. (a) is α'' crystallinity compared with crystal orientation and (b) is α'' crystallinity compared with amorphous orientation. The units of *Y*-axes are relative units just for comparing the changing trends. (○: Orientation, □: α'' phase crystallinities). [Color figure can be viewed in the online issue, which is available at wileyonlinelibrary.com.]

Deformation-Induced Phase Transition

Like other semicrystalline polymers, there also shows crystal-to-crystal transition in PA12 film during tensile deformation.[29,31] Because γ phase is the most stable form in the film, and the whole tensile experiments were done at room temperature, the most crystal phase in the sample at first is γ phase, which is verified by the FTIR spectra as shown in Figure 5. For undeformed PA12 samples, the 946 cm^{-1} band (CONH in-plane deformation) in the spectrum belongs to the γ phase while 1160 cm^{-1} band (Skeletal motion involving CONH deformation) belongs to the amorphous phase.[42] Because there have large numbers of hydrogen bonds and some are perpendicular to the stretching direction, these cause the two bands not showing strong dichroism. Because the two bands show strong infrared absorption behaviors and are easy to find the shape changes during tensile deformation, the 946 and 1160 cm^{-1} bands are selected for crystal-to-crystal transformation analysis.

After giving a detailed analysis of the spectra in the fingerprint region (1200–900 cm^{-1}), there have not any changes of the amorphous band at 1160 cm^{-1} during whole tensile deformation (the band intensities decreasing mainly come from the sample thinning during drawing), but the crystal band at 946 cm^{-1} shows with certain complexity during the process. In the elastic region (as shown the fast increasing region in the engineering stress–strain curve [Figure 1 (b)], there can not find any changes of the crystal band. After yielding (the corresponding spectrum is denoted with the short dash line), a small shoulder at 936 cm^{-1} appears, which belongs to the CONH in-plane deformation of α phase and means that other phase with structures similar to α phase forming during tensile deformation in plastic stage. Because α crystal in PA12 forms under deformation at temperatures close to the melting point, we can not directly assign this deformation-induced phase as α crystal. Following X-ray diffraction results of our early work, the new phase is denoted as α'' crystal.[29,31]

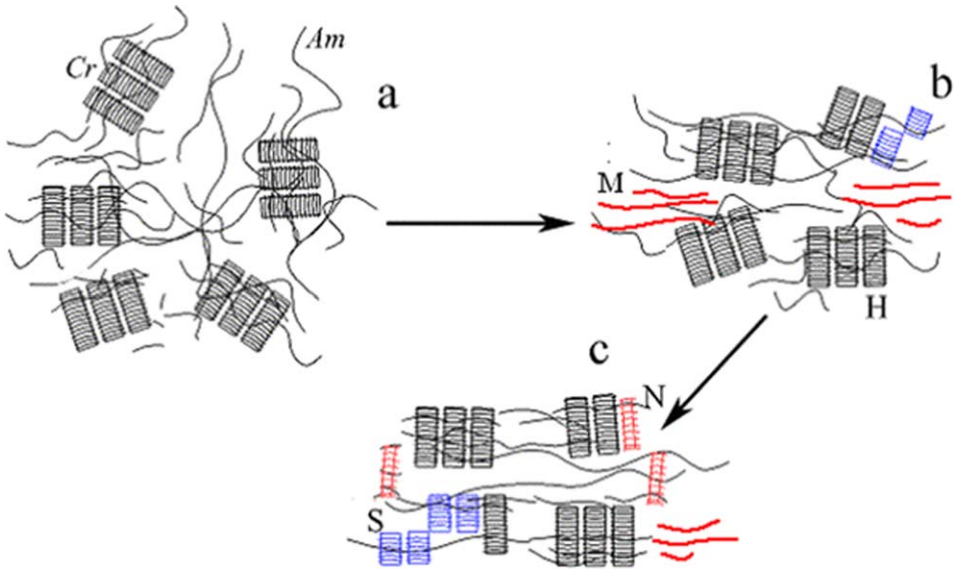

Figure 10. Schematic diagrams of the deformation process under uniaxial stretching. The morphology before stretching (a) during stretching (b), and the final stable morphology (c). N represents new form crystal, S represents slipping crystal, M (with red lines) represents melting crystal, and H represents orientated crystal. [Color figure can be viewed in the online issue, which is available at wileyonlinelibrary.com.]

Considered that the overlap with 946 cm^{-1}, a lorentzian fitting is adopted to obtain the real intensity of 936 cm^{-1} band with Matlab software. To simplify the analysis, we assume that the infrared absorption coefficients of γ and α'' crystals are same, then the values of the contributions of the γ and α'' crystals can be calculated using the integrated intensities of fitting curves of the two crystals of A_γ or $A_{\alpha''}/(A_{\text{crystal}}+A_{\text{amorphous}})$, where A_{crystal} is the integrated intensity of γ and α'' crystal band. The fitting curves with different strains are shown in Figure 6. The estimated γ and α'' crystallinities in 250 × 250 μm^2 microzone in the necking region can be calculated and the corresponding selected 2D crystallinity images and average distributions along the neck propagating direction can be obtained (as shown in Figures 7 and 8). Because there almost have no changes of the crystal spectral band under deformation in the elastic region, no new crystal phase is considered to form during this period. But after yielding ($\varepsilon > 1.0$), a new small 936 cm^{-1} shoulder appears and the intensities increase with the strain increasing, which means that α'' phase begins to develop in plastic deformation stage.

The 2D distributions of α'', γ crystallinities and average α'', γ crystallinities in the necking region along tensile deformation are presented in Figures 7 and 8. The figures indicate that, α'' phase mainly forms in the necking region, the new phase distribution expands as the neck propagating and the crystallinities increase with strain increasing. At the same time, the γ crystallinities show opposite changes as the neck propagating during drawing. There have about 2.3% of maximum α'' crystallinities increasing and about 3.4% of maximum γ crystallinities decreasing in the detected region during tensile deformation. The difference of α'', γ phase changing is that α'' crystallinitiy continuously increases while γ crystallinity almost keep in a constant at high drawing as the neck expanding to the whole detected region. The results reveal that γ transits to α'' phase during neck initiating and propagating and also other phases transform to crystal phase in plastic deformation stage, which compensate part of consumed γ phase. The average ratios of $C_{\alpha''}/C_\gamma$ also show the same crystal changing trends in the necking region.

To evaluate the correlation of γ and α'' phase transformation during tensile deformation, the average changing trends of α'' crystal compared with the crystal and amorphous orientations in necking region are presented in Figure 9 (a,b). In the figures, α''crystallinities and crystal orientation distributions are almost uniform before neck initiating. When neck forming and propagating (strain > 0.7), α'' crystal increasing is almost consistent with that of crystal and amorphous orientations in the necking region. The faster the crystal and amorphous orientation increases, the more the phase transition occurs. The difference of amorphous and crystal increasing is that there has a slight decrease of amorphous orientation while crystal orientation continuously increasing at high strains.

As discussed above, amorphous phase will transform to crystal phase during tensile deformation, and the calculated γ and α'' crystallinities also reveal that γ phase decreasing more slowly than α'' phase increasing at high-drawing ratios, which indicate that the probability of amorphous phase transforming to γ phase is larger than that of amorphous phase to α'' phase, and the new forming γ phase compensates part of the one transforming to α'' phase, thus the γ phase decreasing to the plateau is earlier than α'' phase increasing to the plateau. Because there have large amounts of hydrogen bonds between the γ sheets as well as inside the γ crystals and the hydrogen bonds between the γ sheets may directly bear the load,[45] new phase could not be developed in the early elastic stage.

In the studies, we discuss that the transient α'' form is always produced in plastic deformation stage and our group has also proved that the appearance of α'' form mainly be caused by martensitic transformation of γ crystal.[29] But the crystallinities

of α'' phase can not increase unlimitedly and finally almost reaches to a plateau as the strain increasing, we can indicate that α'' form is unstable and will transform to mesomorphic state during tensile deformation. The results show that the yielding and necking behaviors of PA12 are strongly correlation with the phase transition processes by various deformations of the crystal and amorphous regions.

The experimental results reveal that there has a distribution of crystal and amorphous orientations along the tensile direction and the crystal orientation increases faster than the amorphous orientations during neck initiating and propagating. Also tensile deformation can induce crystal-to-crystal and amorphous-to-crystal transitions in plastic deformation stage. A schematic illustration of this process is presented in Figure 10. The starting sample has an isotropic morphology, where lamellar stacks and interstacks construct a 3D network to sustain stress during tensile deformation [Figure 10 (a)]. During necking propagation, parts of crystals are damaged either through crystal slip or melting, while large numbers of crystals change their orientation through rotation. Because the structures in amorphous region are more incompact and the hydrogen bonds in the region are more dynamic than those in crystal region, these cause crystal orientations increasing faster than amorphous orientations increasing during neck initiating and propagating [Figure 10 (b)]. With the strain continually increasing, the crystal and amorphous phases are highly orientated. Meanwhile, some damaged γ phase will transform to α'' phase as well as amorphous phase transform to crystal phase [Figure 10 (c)].

CONCLUSIONS

The yielding and necking properties as well as the orientation distributions of crystal and amorphous phases are studied by *in situ* FTIRI technique. The studies show that part of amorphous phase transforms to crystal phase during tensile deformation and the new crystal phase with structures similar to α phase develops during neck propagating, there has a quick increase of the crystal and amorphous orientation distributions in the necking region and the distributions expand with the neck propagating. All these indicate that mechanical responses and superstructures of polymers correlate directly with phase transition and necking propagation during uniaxial tensile deformation.

ACKNOWLEDGMENTS

This work is supported by the National Natural Science Foundation of China (51325301, 51033004, 51120135002, U1232128), 973 program of MOST (2010CB934504). The research is also in part supported by China Postdoctoral Science Foundation (Grant No: 2012M521233), "the Fundamental Research Funds for the Central Universities," and the Opening Project of the State Key Laboratory of Polymer Physic and Chemistry (Changchun Institute of Applied Chemistry, CAS). The experiment is carried out in National Synchrotron Radiation Lab (NSRL).

REFERENCES

1. Liang, J. Z. *J. Appl. Polym. Sci.* **2002**, *83*, 1547.
2. Zou, H.; Wu, S.; Shen, J. *Chem. Rev.* **2008**, *108*, 3893.
3. Dencheva, N.; Denchev, Z.; Oliveira, J.; Funari, S. *J. Appl. Polym. Sci.* **2007**, *103*, 2242.
4. Zhang, X. K.; Yang, G. S.; Lin, J. P. *J. Appl. Polym. Sci.* **2006**, *102*, 5483.
5. Wang, B.; Hu, G.; Zhao, X. *Mater. Sci.* **2006**, *60*, 21.
6. Nair, S.; Ramesh, C.; Tashiro, K. *Macromolecules* **2006**, *39*, 2841.
7. Zhang, Y. Z.; Zhang, L.; Liu, S. W. *J. Appl. Polym. Sci.* **2011**, *120*, 1885.
8. Du, L. B.; Yang, G. S. *Polym. Eng. Sci.* **2010**, *50*, 1178.
9. Skrovanek, D. J.; Painter, P. C.; Coleman, M. M. *Macromolecules* **1986**, *19*, 699.
10. Skrovanek, D. J.; Howe, S. E.; Painter, P. C.; Coleman. M. M. *Macromolecules* **1985**, *18*, 1676.
11. Kelnar, I.; Kratochvil, J.; Mikesova, J. *J. Appl. Polym. Sci.* **2007**, *106*, 3387.
12. Leonov, A.I. *Int. J. Solids Struct.* **2002**, *39*, 5913.
13. Nitta, K. H.; Takayanagi, M. *Polym. J.* **2006**, *38*, 757.
14. Hao, C.; Zhao, Y.; Li, W.; Xu, Y.; Wang, D.; Xu, D. *Spectrosc. Spec. Anal.* **2008**, *28*, 2048.
15. Liu, L.; Ren, Y.; Li, Y.; Liang, Y. *Polymer* **2013**, *54*, 5250.
16. Song, Y. H.; Nemoto, N. *Polymer* **2005**, *46*, 6522.
17. Song, Y. H.; Yamamoto, H.; Nemoto, N. *Macromolecules* **2004**, *37*, 6219.
18. Men, Y.; Rieger, J.; Strobl, G. *Phys. Rev. Lett.* **2003**, *91*, 95502/95501–95504.
19. Meijer, H. E.; Govaert, L. E. *Prog. Polym. Sci.* **2005**, *30*, 915.
20. Zhong, G. J.; Li, Z. M.; Li, L. B.; Shen, K. Z. *Polymer* **2008**, *49*, 4271.
21. Zhong, G. J.; Li, Z. M.; Li, L. B.; Mendes, E. *Polymer* **2007**, *48*, 1729.
22. Starkweather, H.; Moore, G.; Hansen, J.; Roder, T.; Brooks, R. *J. Polym. Sci.* **1956**, *21*, 189.
23. Na, B.; Xu, W. F.; Lv, R. H.; Li, Z. J.; Xu, W. F.; Fu, Q. *Macromolecules* **2010**, *43*, 3911.
24. Na, B.; Lv, R. H.; Tian, N. N.; Xu, W. F.; Li, Z. J.; Fu, Q. *J. Polym. Sci. Part B: Polym. Phys.* **2009**, *47*, 898.
25. Pierron, L.; Seguela, R.; Lefebvre, J.; Miri, V.; Depecker, C.; Jutigny, M.; Pabiot, J. *J. Polym. Sci. Part B: Polym. Phys.* **2001**, *39*, 1224.
26. Vasanthan, N. J. *Polym. Sci. Part B: Polym. Phys.* **2003**, *41*, 2870.
27. Ishikawa, T.; Nagai, S.; Kasai, N. *Makromol. Chem.* **1981**, *182*, 977.
28. Wan, C.; Zhao, F.; Bao, X.; Kandasubramanian, B.; Duggan, M. *J. Polym. Sci. Part B: Polym. Phys.* **2009**, *47*, 121.
29. Wang, D. L.; Shao, C. H.; Zhao, B. J.; Bai, L. G.; Wang, X.; Yan, T. Z.; Li, J. J.; Pan, G. Q.; Li, L. B. *Macromolecules* **2010**, *43*, 2406.
30. Li, L. B.; Koch, M. H.; de Jeu, W. H. *Macromolecules* **2003**, *36*, 1626.
31. Bai, L. G.; Hong, Z. H.; Wang, D. L.; Li, J. J.; Wang, X.; Pan, G. Q.; Li, L. B.; Li, X. H. *Polymer* **2010**, *51*, 5604.

32. Hong, Z. H.; Cong, Y. H.; Qi, Z. M.; Li, H. L.; Zhou, W. M.; Chen, W.; Wang, X.; Zhou, Y. G.; Li, L. B. *Polymer* **2012**, *53*, 640.

33. Li, H. L.; Zhou, W. M.; Ji, Y. X.; Hong, Z. H.; Miao, B.; Li, X. Y.; Zhang, J.; Qi, Z. M.; Wang, X.; Li, L. B. *Polymer* **2013**, *54*, 972.

34. Li, J.; Li, H. L.; Meng, L. P. *Polymer*, submitted.

35. Wen, S.; Zhou, Y.; Yao, L.; Zhang, L. Q.; Chan, T. W.; Liang, Y. R.; Liu, L. *Thermochim. Acta* **2013**, *571*, 15.

36. Ishisue, T.; Okamoto, M.; Tashiro, K. *Polymer* **2010**, *51*, 5585.

37. Vidal, B. *Acta Histochem.* **2013**, *115*, 686.

38. Ling, S. J.; Qi, Z. M.; Knight, D. P.; Huang, Y. F.; Huang, L.; Zhou, H.; Shao, Z. Z.; Chen, X. *Biomacromolecules* **2013**, *14*, 1885.

39. Galimberti, D.; Quarti, C.; Milani, A.; Brambilla, L.; Civalleri, B; Castiglioni, C. *Vib. Spectrosc.* **2013**, *66*, 83.

40. Luo, J.; Zhou, T.; Fu, X.; Liang, H. W.; Zhang, A. M. *Eur. Polym. J.* **2011**, *47*, 230.

41. Cui, X. W.; Yan. D. Y. *Eur. Polym. J.* **2005**, *41*, 863.

42. Xiao, Y.; Zhu, X. Y.; Chen, L.; He, P.; Yan, D. Y.; Wang, X. G. *J. Polym. Sci. Part B: Polym. Phys.* **2003**, *42*, 60.

43. Rhee, S.; White, J. L. *J. Polym. Sci. Part B: Polym. Phys.* **2002**, *40*, 1189.

44. Parthasarthy, G.; Sevegney, M.; Kannan, R. M. *J. Polym. Sci. Part B: Polym. Phys.* **2002**, *40*, 2539.

45. Skrovanek, D.; Painter, P.; Coleman, M. *Macromolecules* **1986**, *19*, 699.